UCRL-ID-148021-REV-2

Thick Liquid-Walled Spheromak Magnetic Fusion Power Plant

R. W. Moir, R. H. Bulmer, T. K. Fowler, T. D. Rognlien, M. Z. Youssef

April 28, 2003

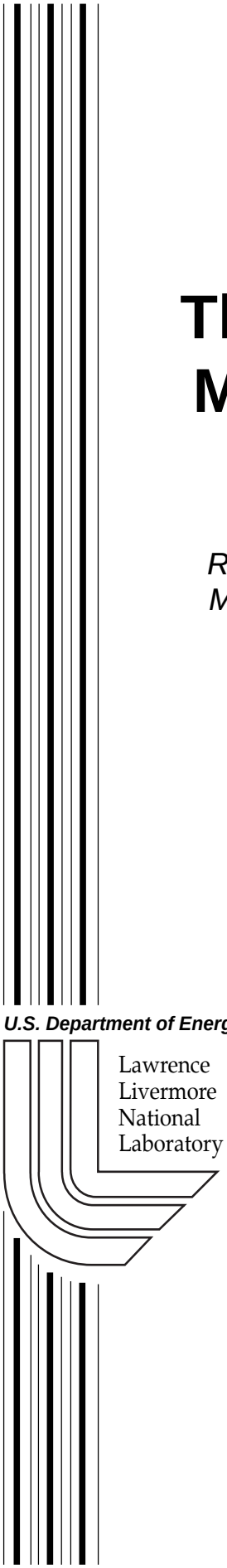

Approved for public release; further dissemination unlimited

This document was prepared as an account of work sponsored by an agency of the United States Government. Neither the United States Government nor the University of California nor any of their employees, makes any warranty, express or implied, or assumes any legal liability or responsibility for the accuracy, completeness, or usefulness of any information, apparatus, product, or process disclosed, or represents that its use would not infringe privately owned rights. Reference herein to any specific commercial product, process, or service by trade name, trademark, manufacturer, or otherwise, does not necessarily constitute or imply its endorsement, recommendation, or favoring by the United States Government or the University of California. The views and opinions of authors expressed herein do not necessarily state or reflect those of the United States Government or the University of California, and shall not be used for advertising or product endorsement purposes.

This work was performed under the auspices of the U.S. Department of Energy by University of California, Lawrence Livermore National Laboratory under Contract W-7405-Eng-48.

Approved for public release; further dissemination unlimited

UCRL-ID-148021 Rev. 2

Thick liquid-walled spheromak magnetic fusion power plant

R. W. Moir, R. H. Bulmer, T. K. Fowler, T. D. Rognlien, M. Z. Youssef

April 28, 2003

Abstract

We assume a spheromak configuration can be made and sustained by a steady plasma gun current, which injects particles, current and magnetic field, i.e., helicity injection. The magnetic configuration is evaluated with an axisymmetric free-boundary equilibrium code, where the current profile is tailored to support an average beta of 10%. An injection current of 100 kA (125 MW of gun power) sustains the toroidal current of 40 MA. The flux linking the gun is $1/1000^{th}$ of the flux in the spheromak. The geometry allows a flow of liquid, either molten salt (flibe–Li_2BeF_4 or flinabe–$LiNaBeF_4$) or liquid metal, such as SnLi, which protects most of the walls and structures from neutron damage. The free surface between the liquid and the burning plasma is heated by bremsstrahlung and optical radiation and neutrons from the plasma. The temperature of the free surface of the liquid is calculated and then the evaporation rate is estimated. The impurity concentration in the burning plasma is estimated and limited to a 20% reduction in the fusion power (≈0.8% fluorine impurity). The divertor power density of 620 MW/m^2 is handled by high-speed (100 m/s) liquid jets. Calculations show that the tritium breeding is adequate with enriched ^6Li and appropriate design of the walls not covered by flowing liquid (15% of the total). A number of problem areas need further study to make the design self consistent and workable, including lowering the divertor power density by expanding the flux tube size.

Table of contents

Introduction and background

This power plant design study applies liquid walls to the steady state spheromak plasma confinement configuration. A self-consistent point design was the goal.

The spheromak idea came about by a number of routes[1]. The toroidal coils of the tokamak might not be necessary if the plasma could carry enough current to make a sufficient toroidal field. In this case, the performance might be tokamak-like with a simpler magnet configuration. Marshall plasma guns made reasonably stable configurations. Early experiments were encouraging. Hagenson and Krakowski made a reactor design [2]. Other reactor studies included solid first walls and boiling liquid blankets [3] and pulsed liquid walls [4]. Physics opportunities and issues of the reactor are discussed in [5]. The main theme of this work is the use of liquid wall and steady state operation.

The logic of this design process follows:

- the configuration is based on MHD equilibrium calculations
- a discussion of the steady-state gun injection for current drive
- the development of the plasma and other related parameters
- a discussion of the electrodes and insulators
- a discussion of the liquid wall flows with the calculation of surface temperatures (based on incident power on the liquid surface and interior,)
- the calculation of evaporation rates from the liquid surfaces that depend only on surface temperature
- discussion of the edge plasma, the estimates of evaporation allowed from core plasma contamination with impurities, and the ability to breed tritium

We consider low conductivity liquids (molten salts) and high conductivity liquids (liquid metals). The usual molten salt is flibe (Li_2BeF_4), but past studies show that evaporation limits require temperatures near or below the melt temperature of 460 °C. Adding NaF to flibe produces flinabe ($NaF+LiF+BeF_2$ =

$LiNaBeF_4$) [6], whose melt temperature is reduced to ~310 °C. This study is based on flinabe as a candidate molten salt. SnLi is the liquid metal candidate.

There are many aspects of the design that need further work. These are discussed through out the report and many suggestions for further work are made.

Configuration-equilibria

The spheromak reactor shown in Fig. 1 was developed with the Corsica code[6a]. It is an axi-symmetric configuration with a nearly up / down symmetrically confined region. A slight vertical asymmetry provides a single (lower) divertor. The shape of the confined region is maintained with 6 circular coils arranged in an up / down symmetric fashion. Two additional coils channel diverted flux around the gun electrodes and into a collector region. The free-boundary equilibrium design has a flux amplification factor of 1000 with an elongation less than 2 to mitigate instabilities. Of particular concern are tilt and shift modes, which will probably require [7] active feedback coils. We envisioned relatively small coils near the inner surface of the shielding structure facing the plasma in the confined region. The outer radius of the confined region is 6 m and the confined volume is 652 m^3.

The distance from the outer edge of the plasma to the first rigid conducting wall is 1 m in the case of flibe (0.5 m from the plasma edge to the low conductivity flibe and 0.5 m of flibe to the 30-mm thick stainless steel wall). In the case of SnLi the conducting liquid wall is 0.5 m from the plasma.

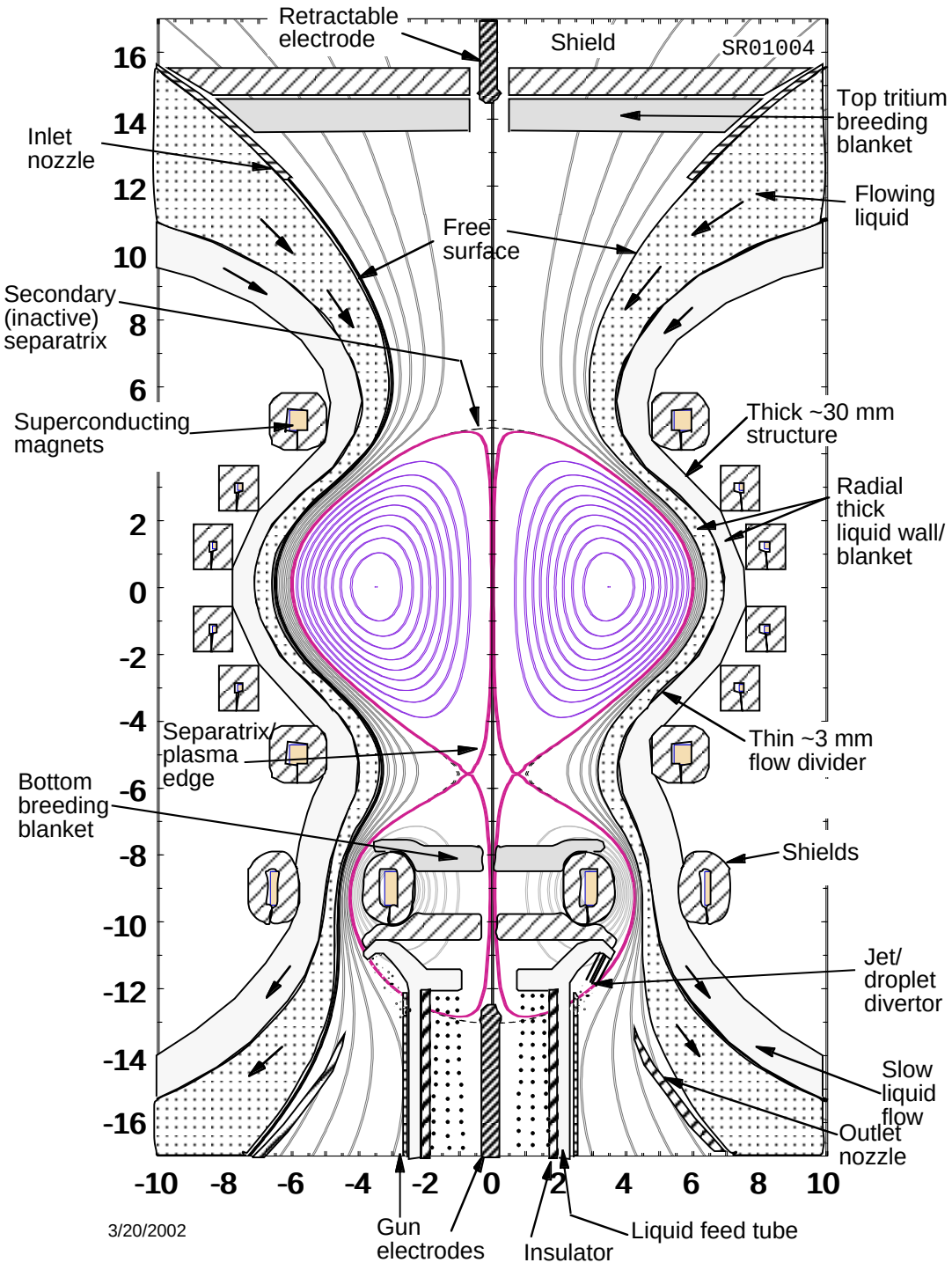

Fig. 1. The spheromak configuration with liquid walls shown above is the subject of this report. The liquid flow is kept to the outside by centrifugal force for molten salt and by magnetic guide field for liquid metals. Liquid jets greatly aid divertor heat removal.

The current profile deviates from the relaxed Taylor-state in that the λ–profile (normalized current density, see [1]):

$$\lambda(\psi) = \frac{\mu_0 \mathbf{j}\cdot\mathbf{B}}{B^2} \qquad (1)$$

varies, as shown in Fig. 2. This creates shear consistent with a Mercier plasma beta limit of $\frac{p}{B^2/2\mu_0} = 0.1$. The value of λ on the open field-lines is about half that at the magnetic axis. The pressure profile, also shown in Fig.2, has been optimized to yield the maximum Mercier limit for the given λ–profile. The *q*-profile ($q = \langle \frac{B_\varphi}{B_z}\frac{r}{R} \rangle$) varies from 0.9 on the magnetic axis to 0.3 near the edge.

The toroidal current is 40 MA, which results in $B_\varphi \approx B_\theta = 2.89$ T at the magnetic axis[1] (magnetic field profiles are shown in Fig. 3). This level of current requires pack current densities of ~30 A/mm^2 in the shaping coils (near a practical limit). The coil sizes are shown in Fig. 1. As noted, the toroidal current will have to increase as the design evolves; the coil currents will increase in direct proportion. Therefore, the coil cross-sectional dimensions will have to increase by about 25% to keep the current densities within limits.

The main equilibrium parameters are summarized in Table 1. Note the gun current in the equilibrium model, 18.2 kA, is significantly less than the 100-kA value discussed later in the gun model section. This discrepancy is due to the particular values of the toroidal current and the ratio of λ_{ext}/λ_0 in the equilibrium model and needs to be resolved as the design evolves.

Another area for future work involves the edge-flux expansion ratio from the midplane to the divertor region. In the present design, the radial distance between the edge of the confined region and the inactive separatrix (Ψ=0 contour) is 1.5 mm and only expands by a factor of 4 to 6 mm in the divertor

[1] This field level is not yet consistent with the total fusion power. The toroidal current will have to be increased to ~60 MA to produce the desired 4.3 T field level if this is the correct field to scale from (see the next section for a discussion of scaling and further work needed).

region. In order to reduce the power density to the divertor, it may be necessary to increase this expansion ratio by a factor of 2 to 12 mm in the divertor region to handle the power flux density discussed in the divertor section. This change will require an adjustment in the current and in the position of the outer divertor coil. Perhaps it will also require an additional divertor coil.

Table 1

Equilibrium parameters

Toroidal current, MA	40
Toroidal B-field (R=3.49 m), T	2.89
Poloidal current (gun), kA	18.2
Poloidal B-field (R=0), T	5.24
Poloidal flux (edge), Wb (R=0 to separatrix)	0.08
Poloidal flux (R-0 to 3.49 m), Wb	75.8
Separatrix radius, inner, m	0.068
Separatrix radius, outer, m	6.00
Magnetic axis radius, m	3.49
Core plasma volume, m^3	652
Core plasma surface, m^2	362
Volume average beta, %	10

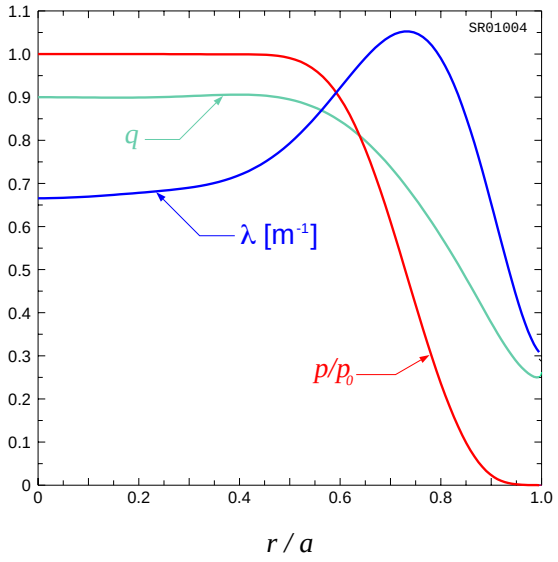

Fig. 2. Profiles of pressure, current (λ) and Safety Factor (q) at the midplane.

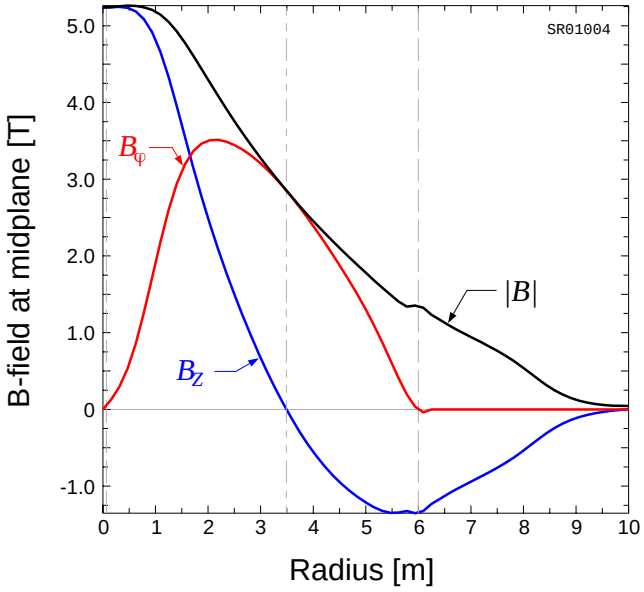

Fig. 3. Magnetic field profile. B_ϕ and B_z are the toroidal and poloidal fields, respectively. The field is consistent with a model having 40 MA toroidal current and beta equal to 10% volume averaged

Plasma parameters

The Corsica model has a plasma pressure giving a volume-averaged beta of 10%. The field of 5.24 T on R=0 axis, which corresponds to a 40 MA toroidal current. Based on prior work on the Field Reversed Configuration (FRC) [8], we can scale

to get a first approximation of some of the parameters. First we scale the power density.

$$\frac{P_{FRC}}{V} = \frac{2500}{2.6} = 961.5 \frac{MW}{m^3} \qquad \text{r=0.39 m separatrix case for FRC for scaling} \qquad (2)$$

$$\frac{P_{Spheromak}}{V} = \frac{2500}{652} = 3.834 \frac{MW}{m^3} \qquad (3)$$

$$\frac{P}{V} \propto n^2 \propto \frac{\beta^2 B^4}{T^2} \qquad (4)$$

The effect of impurities diluting the fuel ions needs to be included in future analyses. We assume in this work that more magnetic field will be provided to hold the increased pressure owing to the impurities and their associated electrons.

$$\frac{(\beta^2 B^4)_{Sph}}{(\beta^2 B^4)_{FRC}} = \frac{3.834}{961.5} = 3.988 \cdot 10^{-3} \qquad (5)$$

From Table 2, we see the FRC field is 5.5 T but this is on the r=0 axis (the field on the magnetic axis is zero for the FRC).

$$B_{Sph} = (3.988 \cdot 10^{-3} \cdot 0.97^2 \cdot 5.5^4 / 0.1^2)^{\frac{1}{4}} = 4.305 T \qquad (6)$$

This value of magnetic field probably corresponds to the value somewhere between the r=0 axis of 2.89 T and that at the magnetic axis of 5.24 T –a reasonable first guess. A better estimate is left to future work.

The plasma fuel ion density is also scaled from the FRC work.

$$n_{Sph} \propto \frac{1}{\sqrt{\frac{P}{V}}} \qquad (7)$$

$$n_{Sph} = 26 \cdot 10^{20} \sqrt{\frac{3.834}{961.5}} = 1.64 \cdot 10^{20} / m^3 \qquad (8)$$

The volume within the last closed flux contour is 652 m^3. The circumference in the poloidal plane of the last flux contour is 24.3 m. The area within this contour in the poloidal plane is 37.9 m^2. The surface area from the separatrix to the upper apex along the inside or nearest the axis is about 23 m^2 and the area on the outside is 362 m^2. This may be useful in deciding how much leakage plasma should enter the divertor on the outside versus the inside. Using the area ratio suggests that the inside plasma leakage is only 6% of the outside leakage. We need to estimate the width of plasma flow on the inside flux surface to estimate the power density there. If we can show the power density on the inside divertor is small, we need only treat the outside divertor (see section on divertor).

Table 2

Typical spheromak power plant parameters.

	Spheromak	FRC	FRC
Liquid wall radius, m	6.5	1.5	2.0
Separatrix radius, m	0.068, 6.0	0.39	1
Magnetic axis, m	3.49	0.29	0.75
Separatrix length, outside and inside, m	15, 10	8	8
Liquid flow path length, inlet nozzle exit nozzle, m	27	14	14
Core plasma volume, m^3	652	2.6	25
Outer plasma area, m^2	362	75	100
Average ion temperature, keV	12	12	18
Average ion density, 10^{20} m^{-3}	1.64	26	6.2
Peak ion density, 10^{20} m^{-3}	?	31	6.8
Z_{eff}	1.5	1.5	1.5
s = plasma radius / average larmor radius	1100	7.5	26
Helicity current drive, kA Helicity (Gun) power, MW	100 125	---	---
Toroidal current, MA	40		40
Volume-averaged beta	0.1	0.97	0.78
Magnetic field, T Poloidal Toroidal	Bz=5.24 @r=0 Bϕ=2.89@r=3.49	5.5	3.6
Flux from r=0 to the separatrix, Wb	0.08	---	---
Flux from separatrix to mag axis, Wb	75.8	---	---
Energy confinement time, s	?	0.08	0.33
Ash particle conf. time, s	?	0.16	0.65
Neutron wall load ave, MW/m^2	5.5	27	18
Surface heat load, MW/m^2	0.47	1.7	1.2
Neutron power, MW	2000	2000	1844
Bremsstrahlung radiation power	60.8 MW, 0.17 MW/m^2	46	49
Line radiation, core	10.7 MW, 0.03 MW/m^2	---	----
Line radiation, edge	7.6 MW, 0.02 MW/m^2	78	69
Power to divertor, MW 500+125-10.7-7.6=546	546	415	383
Input (Gun) power, MW	125 @ Q=20	40	40
Fusion power, MW	2500	2500	2306
Net electric power, MWe	~1000	1000	1000

Radiation model

The assumed values for radiation used in this report are given in Table 2 above and in Table 4. At an electron temperature of 12 keV, impurities from flibe will be mostly in the highest charge state and, therefore, will produce little line radiation. However, near the lower temperature edge region there will be increased line radiation. The radiation from the core will consist of about 85% bremsstrahlung radiation and about 15% line radiation (see Fig. 4.10.1 of ref. 9). From Fig. 4.10.2 of [9], we see that when the ratio of density of fluorine (the most important flibe impurity) to hydrogen ions is 0.03, the radiation will be 10% of the fusion power, or 50% of the alpha power.
From Ref. 9, p 103 we get the equation:

$$F = \frac{(1 + f\bar{Z})\, fR}{\frac{1}{4}\langle \sigma v \rangle E}$$

F=0.1 (radiation is 10% of the fusion power) at an impurity fraction, f, of 0.03 for 10 keV fluorine with $\bar{Z}$=9. From these values we get $\frac{fR}{\frac{1}{4}\langle \sigma v \rangle E}$ = 2.6247. For an impurity fraction, f, of 0.01, the radiation fraction F is 0.0286 times the fusion power, or 0.143 time the alpha power.

Thus, when the ratio of flibe impurities to fuel ions is 0.01, the radiation will be 14.3% of the alpha power. This would amount to 71.5 MW (85% or 60.8 MW of bremsstrahlung and 15% or 10.7 MW of line radiation from the core). This is more than a factor of three lower than 50% due to the non-linear term in the equation on p 103 of [9]. If we desire to enhance radiation from the core to the liquid wall, a small amount of added impurity with a Z much higher than that of fluorine (Z=9) would give the desired radiation. This assumes enough power to maintain the electron temperature.

We also considered fuel dilution from the fluorine; a 0.03 fraction of fluorine reduces the fusion power by an additional 38% if the total ion density is fixed.

In the edge plasma, or scrape off layer (SOL), where the electron temperature may be lower than 1 keV, the fluorine will be in partially ionized states and produce mostly line radiation. Estimates can be made for this line radiation, expressed as a fraction of the alpha power. In the divertor region, where recycling between gaseous and ionized states is occurring, considerable line radiation will occur. The line radiation merely spreads the plasma power over more liquid in the localized divertor region. This power will produce evaporation of the liquid, whose impurity ions will be partially shielded from the core plasma owing to its localization in the divertor region. Nevertheless, some of these impurities will penetrate to the core, and specific transport calculations are needed for a quantitative assessment.

For the UEDGE simulations of the edge plasma, the line radiation from fluorine in the scrape-off layer (SOL) is 1.9% of the alpha power, or 9.5 MW when the fluorine level at the core boundary is 1% of the D-T density there (taken to be 5×10^{19} m^{-3}). The edge line radiation is proportional to impurity density in this low-recycle regime. Approximately 80% of this 9.5 MW or 7.6 MW falls on the liquid wall and 1.9 MW is localized to the divertor region. If the fluorine concentration remains constant in the core at 1% the fusion power is reduced by 16% owing to fuel dilution. There is evidence from tokamak experiments that the impurity concentration at the core edge can be larger than in the central core in some circumstances that would allow a larger edge fluorine fraction. In addition, the low radiation fraction from the SOL is due in part to the low edge density assumed, which in turn comes from the assumption of a low-recycling divertor.

Current Drive Model

The magnetized Marshall gun used to create and sustain spheromaks can be represented by an electric circuit in which the helicity injection impedance is approximated by a resistor, R_S, giving a total gun impedance [10]:

$$R_{GUN} = (5T/I) + R_{FC} + R_S \qquad (9)$$

where I is the gun current; 5T is the approximate sheath voltage with temperature T (in eV) in the "flux core" that guides the gun bias flux and current along the geometric axis of the machine; and R_{FC} is the ohmic resistance in the flux core. Only R_S is useful in sustaining the spheromak, with an efficiency, f, giving as the requirement for steady state:

$$fI^2R_S = P_\Omega = E/\tau = 14\ \text{MW} \qquad (10)$$

where P_Ω is the ohmic dissipation of the spheromak with magnetic energy E and decay time, τ, that we estimate as E = 700 MJ and τ = 50 s for the parameters in Table 2. Finally, an optimum efficiency of f = 0.5 is obtained for a gun current given by [10,11]:

$$I = f^{-1}(5/R\mu_o)\psi = 100\ \text{kA} \qquad (11)$$

where 5/R is the lowest Taylor eigenvalue for flux conserver radius R = 6m for the design shown here and flux core ψ = 0.08 W (the flux between r=0 and the separatrix). Scaling from SSPX gives T = 50 eV and R_{FC} = 1.4 mΩ if we take an effective length $\approx$ R along the geometric axis in the confinement region where the magnetic field B is highest and the cross-sectional area of the flux core (= ψ/B) is smallest [10].

The above formulas give the gun parameters in Table 3, which in turn give those of Table 2.

Table 3.

Gun Parameters

Gun Current, I (kA)	100
Helicity injection impedance, R_S (mΩ)	2.8
Total gun impedance, R_{GUN} (mΩ)	6.7
Gun voltage, I R_{GUN} (V)	670
Power consumed by the gun, I^2R_{GUN} (MW)	67
Gun power supply power, P (MW)	125

Limiting the gun power to 125 MW, to produce the nominal fusion gain Q = 20 in Table 2, requires a total impedance P / I = 12.5 mΩ. This calls for a not-unreasonable d.c. power supply impedance 12.5 - 6.7 = 5.8 mΩ and an overall efficiency to sustain the spheromak = P_Ω / P = 14 / 125 = 11%.

The unknown physics resides in the helicity injection impedance R_S–the subject of ongoing research in SSPX. The required value R_S = 2.8 mΩ in Table 3 is consistent with an enhanced resistance model of SSPX results, giving [10]:

$$R_S = f(1 - f^2)(\alpha\beta)\, R_{FC} = 2.5\ m\Omega \qquad (12)$$

with f = 0.5 as above and αβ = 4.8 to fix SSPX data [10]. The actual impedance may be higher, giving somewhat different bias flux and current, greater efficiency, and higher Q (e.g. $R_S \approx 10$ mΩ in earlier CTX results at Los Alamos [9]). The larger question is whether the instability processes of magnetic tearing and reconnection–thought to underlie the helicity injection impedance characteristic of short pulse experiments to date (milliseconds)–will persist in steady state.

Electrode design

The electrodes shown at the bottom of Fig. 1 provide the 100 kA of helicity current drive. Its active area is a disk of about 0.25 m radius. This gives a current density of 50 A / cm^2. A tapered electrode could reduce this current density and might ease cooling

Insulator design

The insulator is a cylindrical sleeve of radius 2 m about 5 m long, shown near the bottom of Fig. 1. Its purpose is to prevent current from passing across the gap between the center electrode at R=0.25 m and the cylindrical electrode at R ≈ 2.2 m. The insulator is shielded from line-of-sight radiation. The neutron and x-ray

dose rates to the insulator from indirect radiation need to be calculated to determine its lifetime.

Power plant considerations

In this section we discuss the power flows following prior studies[12]. We assume 2500 MW of fusion power. Of this, 2000 MW is in the form of 14 MeV neutrons. Nuclear reactions in the flinabe blanket are assumed to multiply this by 1.18, giving 2360 MW thermal power in the blanket. To this we add the incident power of the 500 MW from alpha energy and the helicity injection power, all of which is absorbed by the flowing fluid either in the walls or in the divertor. We assume a case with $Q=P_{fusion}/P_{injection}=20$, so $P_{injection}=125$ MW. The total power going into the flowing fluid is 2985 MW.

2360 MW nuclear power in the blanket
500 MW alpha power
125 MW injection power
2985 MW total

The volumetric flow rate ($\dot{V}$) is given by the flow speed of 10 m/s at the midplane with a 0.5 m thickness. The volumetric flow in the divertor jets and the slow flow in the back of the blanket are small compared to this.

$$\dot{V} = AV = 2\pi r \Delta r v = 2\pi 6.5 \cdot 0.5 \cdot 10 = 204.2\ m^3/s \quad (13)$$

For flibe:

The mass flow rate (see Fig. 5) is:

$$\dot{m}_{blanket} = 2000\,kg/m^3 \cdot 204.2\,m^3/s = 4.084 \cdot 10^5\ kg/s = \text{flow through the blanket} \quad (14)$$

The temperature increase in the mixed flow from inlet to outlet is:

$$\Delta T_{blanket} = \frac{P}{C\dot{m}_{blanket}} = \frac{2985\ MW}{2380\ J\,kg^{-1}K^{-1} \cdot 4.084 \cdot 10^5\,kg/s} = 3.071K \quad (15)$$

Past studies suggest a 100 °C temperature drop in the coolant to and from the heat exchangers is acceptable from an economic standpoint. We desire lower temperatures and use only 50 °C, to keep the surface temperature low. This assumption will result in a modest plant cost increase.

$$\dot{m}_{HX} = \frac{P}{C\,\Delta T} = \frac{2985\,MW}{2380\,J\,kg^{-1}\,K^{-1}\,50\,K} = 2.5084\cdot 10^{4}\,kg/s = \text{flow to heat exchanger} \quad (16)$$

Since the blanket flow rate is larger than the flow to the heat exchanger, a fraction of the flow will be bypassed to the heat exchanger.

$$\dot{m}_{bypass} = \dot{m}_{blanket} - \dot{m}_{HX} = 4.084\cdot 10^{5}\ kg/s - 2.5084\cdot 10^{4}\ kg/s = 3.833\cdot 10^{5}\,kg/s \quad (17)$$

The temperature of the flow to the heat exchanger is assumed to be 450 °C and 400 °C for the flow out. The melt temperature is estimated at 350 °C (perhaps as low as 310 °) for flinabe, giving a small margin (50 °C). Flibe has a melt temperature of 460 °C.

For SnLi:

The mass flow rate (see Fig. 5) is:

$$\dot{m}_{blanket} = 6000\,kg/m^{3}\cdot 204.2\,m^{3}/s = 12.25\cdot 10^{5}\ kg/s = \text{flow through blanket} \quad (18)$$

The temperature increase in the mixed flow from inlet to outlet is:

$$\Delta T_{blanket} = \frac{P}{C\,\dot{m}_{blanket}} = \frac{2985\ MW}{318.1\ J\,kg^{-1}K^{-1}\cdot 12.25\cdot 10^{5}\,kg/s} = 7.659\,K \quad (19)$$

$$\dot{m}_{HX} = \frac{P}{C\,\Delta T} = \frac{2985\,MW}{318.1\,J\,kg^{-1}\,K^{-1}\,100\,K} = 0.9384\cdot 10^{5}\,kg/s \quad (20)$$

Since the blanket flow rate is larger than the flow rate to the heat exchanger, a fraction of the flow will be bypassed to the heat exchanger.

$$\dot{m}_{bypass} = \dot{m}_{blanket} - \dot{m}_{HX} = 12.25\cdot 10^{5}\ kg/s - 0.9384\cdot 10^{5}\ kg/s = 11.31\cdot 10^{5}\,kg/s \quad (21)$$

For Li:

The mass flow rate (see Fig. 5) is:

$$\dot{m}_{blanket} = 485\,kg/m^{3}\cdot 204.2\,m^{3}/s = 0.9904\cdot 10^{5}\ kg/s = \text{flow through blanket} \quad (22)$$

The temperature increase in the mixed flow from inlet to outlet is:

$$\Delta T_{blanket} = \frac{P}{C} = \frac{2985\ MW}{4200\ J\,kg^{-1}K^{-1}\cdot 0.9904\cdot 10^{5}\,kg/s} = 7.176\,K \quad (23)$$

$$\dot{m}_{HX} = \frac{P}{C\,\Delta T} = \frac{2985\,MW}{4200\,J\,kg^{-1}\,K^{-1}\,50\,K} = 1.421\cdot 10^{4}\,kg/s \quad (24)$$

Since the blanket flow rate is larger than the flow rate to the heat exchanger, a fraction of the flow will be bypassed to the heat exchanger.

$$\dot{m}_{bypass} = \dot{m}_{blanket} - \dot{m}_{HX} = 0.99037 \cdot 10^5\ kg/s - 1.421 \cdot 10^4\ kg/s = 8.482 \cdot 10^4\ kg/s \qquad (25)$$

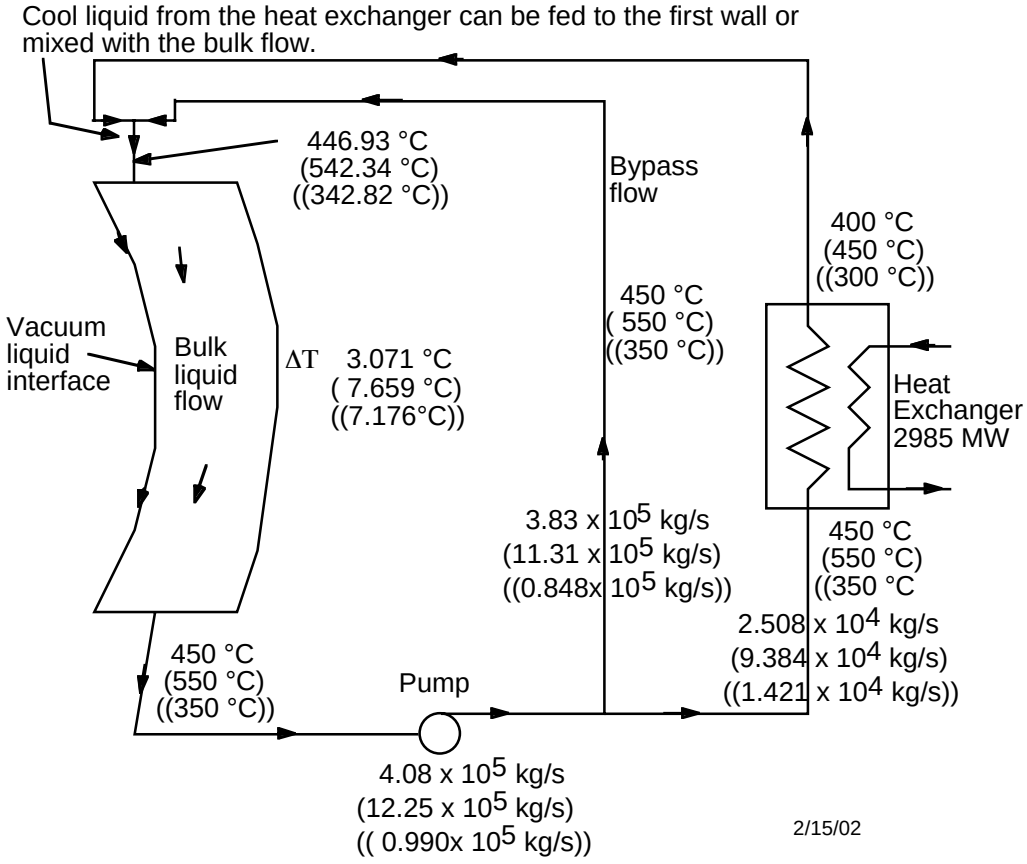

Fig 4. Mass flow and temperature diagram for flibe as the liquid wall. Numbers in parentheses are for SnLi and double parentheses are for Li.

Issues for flibe / flinabe case:

1-ΔT=50 °C across heat exchanger is low. There will be an economic penalty for having so low a value (100 °C is customary).

2-T_{cold} = 400 °C is close to the melt temperature, assumed to be 350 °C. Freeze-up will be an operational issue. Perhaps the melt temperature will be 310 °C and the temperature can be lowered somewhat.

3- T_{hot} = 450 °C is low for Carnot efficiency, so there will be an economic penalty (650 °C is customary).

Issues for SnLi case:

These seem reasonable from power plant point of view.

Issues for Li case:

1-ΔT=50 °C across heat exchanger is low. There will be an economic penalty for having so low a value 100 °C is usual).

2- T_{hot} = 350 °C is low for Carnot efficiency, so there will be an economic penalty (550 °C is customary for a liquid metal system).

Liquid wall design

The liquid flows in from the top in Fig. 1 with a nominal downward speed of 10 m/s. In the case of flinabe there is also an azimuthal speed of about 10 m/s to keep the liquid on the outer wall by centrifugal force, as shown by K. Gulec in related prior studies [Ref. 12, p 5-94 to 5-105]. In the case of SnLi and Li, we assume the magnetic field will keep the flow closely following field lines. Stability of liquid metal flow is an area needing study. To compensate for gravitational acceleration and the resulting reduced thickness of the flowing liquid, we can start with excess thickness. Flow baffles can also slow the flow.

The bulk of the liquid is heated mostly by neutrons by only 3° C for flinabe, 7.7° C for SnLi and 7.2° C for Li cases, as shown in Fig. 4. The line radiation from the core interior and the edge plasma and bremsstrahlung radiation from the core heat the liquid near the surface. We need to determine the surface temperature in order to calculate the evaporation rate.

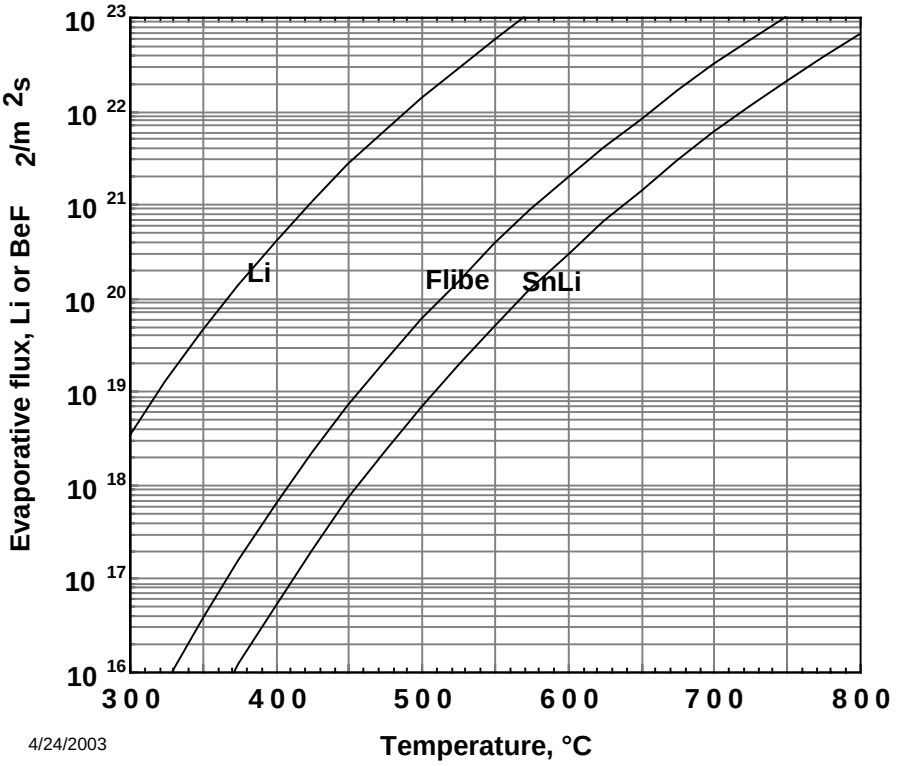

Fig. 5. Evaporation rates into vacuum for candidate liquids based on Ref. 12 p 8-14 to 8-18. The values given are based on data at high temperatures ~1000 °C and extrapolated to lower temperatures. They may be high, especially in the case of flibe.

The vapor pressure for Li_2BeF_4 was $P(Torr) = 10^{9.00045 - 10441.05/T}$ from [13] Cantor, Hsu and Ward (1965). New theoretical analysis lowers the predicted vapor pressure at 500 °C by about a factor of two [14] (Olander, Fukuda, and Baes, Jr., 2002). Adding NaF to flibe will lower the vapor pressure further owing to dilution of BeF_2, and allow the inlet liquid to operate at a lower temperature. This is due to the lower melt temperature of flinabe [6] (Peterson, 2001). These effects were not included in the present work.

The evaporation rate is calculated from the following equations and plotted in Fig. 5.:

$$J = \frac{n\bar{v}}{4}, \quad \bar{v} = \sqrt{\frac{8kT}{\pi m}}, \quad n = \frac{p}{kT}, \quad J = \frac{p}{kT}\frac{\sqrt{\frac{8kT}{\pi m}}}{4} = \frac{p}{(2\pi mkT)^{0.5}}$$

$p = e^{(A-B/T)}$ $J = CT^{-0.5}e^{(A-B/T)}$

$p(Pa) = \exp(25.63 - 24040/T)$.....$Li_2BeF_4$....$BeF_2$ *evaporation* C=3.828x10^{23}

$p(Pa) = \exp(23.29 - 18750/T)$.....*Li*.....*Li evaporation* C=9.961x10^{23}

$p(Pa) = \exp(24.81 - 25800/T)$.....$Sn_{80}Li_{20}$....*Li evaporation* C=9.961x10^{23}

The Li vapor pressure data used in Ref. 8 was in error.

From Table 4, we get 0.05 MW / m^2 of line radiation, surface heat load and 0.17 MW / m^2 of bremsstrahlung radiation. For SnLi, the surface heat load is assumed to be the same as for the flibe case, 0.22 MW / m^2. Photons of 10 keV penetrate ~ 1 mm into flibe, whereas the film thickness is about 8 mm thick.

Table 4

Liquid wall power flux and temperature parameters

Type of power	MW	MW / m^2
Brem.	60.8	0.17
Line, core	10.7	0.03
Line, edge	7.6	0.02
Line, total	18.3	0.05
Total	79.1	0.22
Charged power to divertor	546 328 to lower divertor	619 28 mm flux tube
Flibe		
ΔT_{film}	17 °C	
$T_{effective}$	466 °C	
SnLi		
ΔT_{film}	38 °C	
$T_{effective}$	577 °C	

The high Reynolds number (highly turbulent) flowing liquid with a free surface has eddies at the surface causing the surface to undulate. The transverse motion

at and near the surface causes mass transport and therefore enhanced heat transfer beyond pure conduction. The equivalent thermal conductivity $k_{equivalent}$ has been calculated by Smolentsev [15], and is based on models discussed in [16]. It is plotted in Fig. 6 for flibe divided by the classical thermal conductivity k, for the flow speed of 10 m/s and 0.5 m thickness. We take k to be 1.06 W m^{-1} K^{-1}. Smolentsev [15] gets an enhancement of thermal conductivity at the free surface of 100. However, we must be cautious about this result because by definition the transverse motion vanishes at the free surface. As we move into the liquid, the eddies are assumed to get larger and heat transfer is enhanced even more by convection. His prediction [15] and the model [16] await experimental confirmation. At the back wall there is a 70 μm laminar layer with no transverse motion. The ratio of $k_{equivalent}$ /k approaches unit at the back wall, as it must. We will assume flinabe and flibe have the same properties.

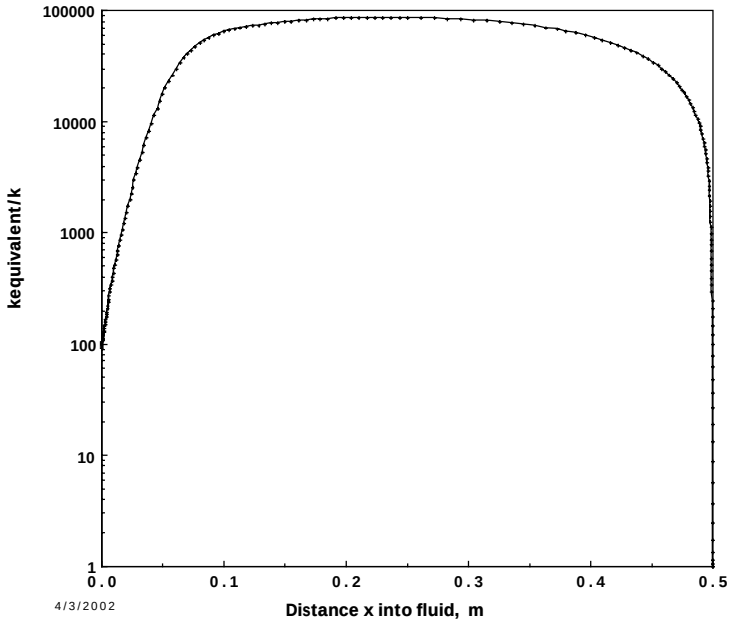

Fig. 6. Thermal conductivity for flinabe and flibe versus distance from the free surface into the flowing liquid.

We obtain the time-averaged temperature profile by integrating the heat conduction equation:

$$\frac{P}{A} = -k_{equivalent}\frac{dT}{dx} \tag{26}$$

where P is the incident power, A, the area, and x the normal distance into the liquid. Rearranging terms:

$$dT = -\frac{P}{k_{equivalent}A}dx \tag{27}$$

Integrating:

$$\Delta T_{film} = T(x=0) - T(x) = -\int_0^x \frac{P}{k_{equivalent}A}dx \tag{28}$$

The integral using the variable equivalent thermal conductivity, from Fig. 6, is plotted in Fig. 7.

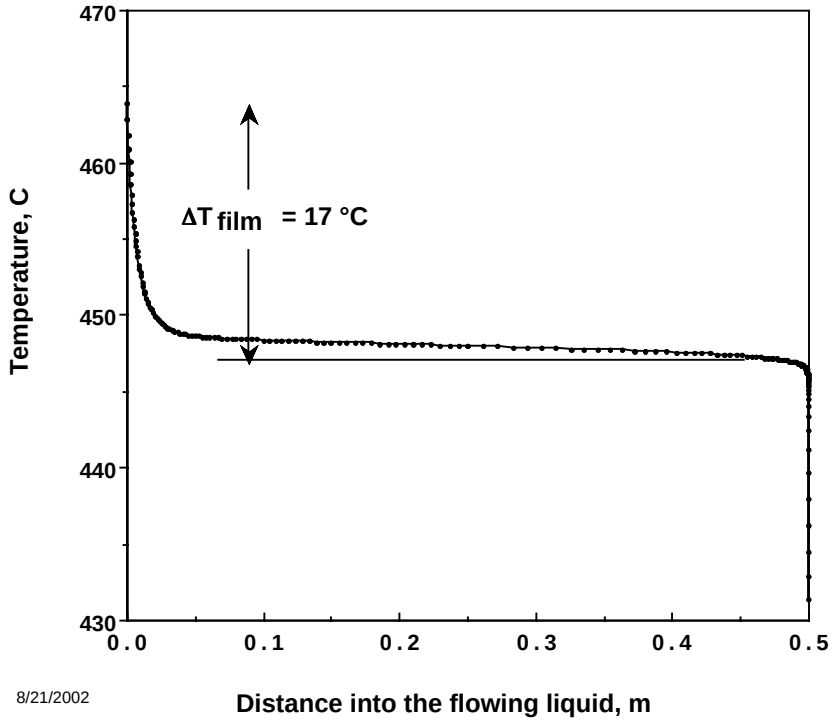

Fig. 7. Temperature profile through the flowing liquid. For a power density of 0.22 MW / m^2 the film drop becomes 17 °C. for flibe flowing at 10 m / s.

There is a film drop on the surface and a flat temperature profile in the very turbulent interior and a film drop on the back wall, which we will ignore because

there is very little heat removal there in our case. Most of the heat is convected out with the flow.

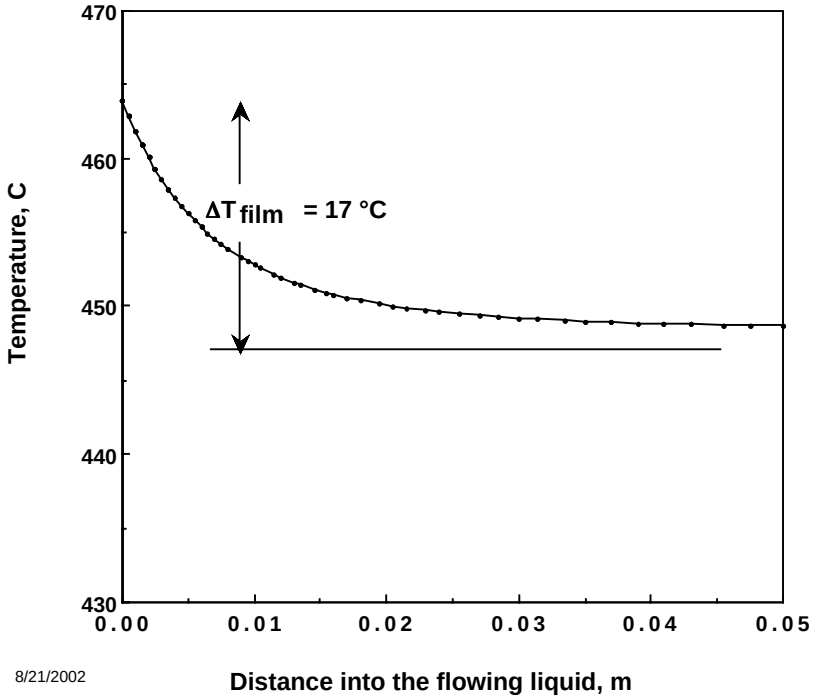

Fig. 8. The temperature profile near the free surface is about 8 mm thick. For a power density of 0.22 MW / m^2 the film drop becomes 17 °C for flibe flowing at 10 m / s.

The temperature drop from the surface to the interior or bulk is approximately 17 °C for this case, with most of this drop occurring in a distance of 8.5 mm. We call this the surface film. It is seen in Fig. 7 & 8.

It may be useful to use the heat transfer coefficient, h, to calculate surface temperature.

$$\frac{P}{A} = h(T_{surface} - T_{bulk}) = h\,\Delta T_{film} \tag{29}$$

$$h = \frac{k_{equivalent}(x=0)\dfrac{dT}{dx}(x=0)}{\Delta T_{film}} \tag{30}$$

From Fig. 7 we get the film drop and from Fig. 8 we get the derivative at the surface, which is then used to calculate the heat transfer coefficient.

$$h = \frac{106\,W/mK\,\dfrac{17K}{0.008\,m}}{17K} = 13{,}250\,\frac{W}{m^2\,K} \qquad (31)$$

Again, this result needs experimental confirmation.

Large eddy analysis

An alternative analysis leads to more pessimistic conclusions based on large eddy formation, which persists even at the free surface. These large eddies are seen in simulations by Kunugi, Satake and Sagara[17]. They predict that the eddies originating from the shear layer near the back wall will grow to be the size of the flow channel thickness [18]. One often see large eddies or boils while on a boat on a river. Lets assume the eddy size is s for flow channel thickness h. The typical speed of the liquid in the eddy at the surface relative to the average surface speed is v'. The surface undulates with these large scale eddies, or boils with the surface moving in the surface film, with the assumed speed for a time to reach the edge of the eddy, t. The configuration is shown in Fig. 9.

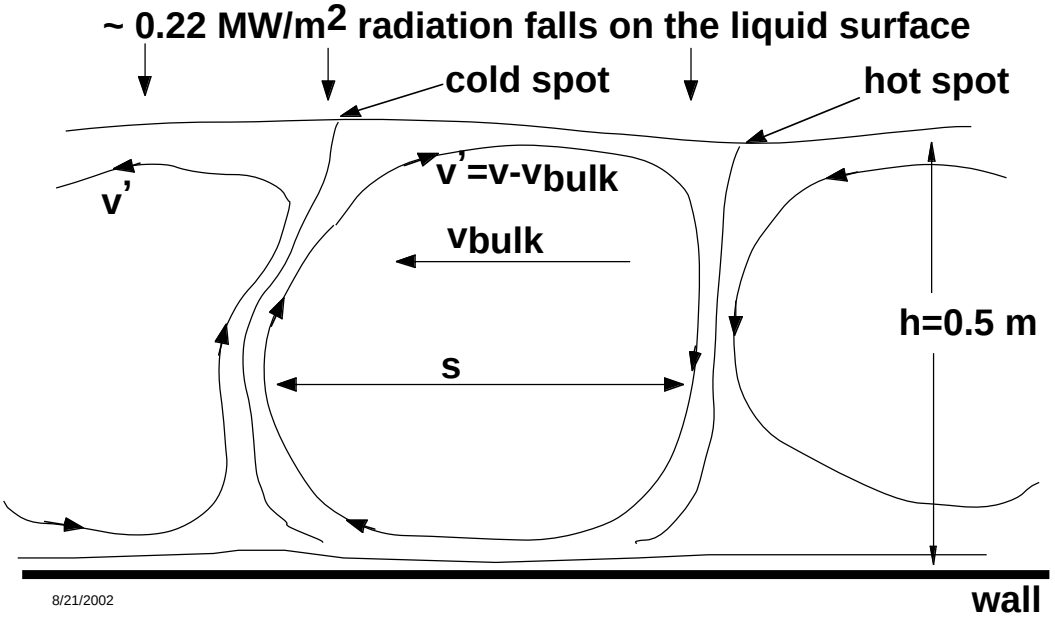

Fig. 9. The configuration for the large eddy analysis is shown with a wavy surface caused by large eddies.

$$t = \frac{s}{v'} = \left(\frac{s}{h}\right)\left(\frac{h}{v_{bulk}}\right)\left(\frac{v_{bulk}}{v'}\right) \qquad (32)$$

As an example, we take the following typical numbers:

$s/h=1$, h=0.5 m, v_{bulk} =10 m/s, v'/v_{bulk}=0.1

then,

t = 0.5 s

$$\Delta T=T_{surface} - T_{bulk}= \Delta T_{film} = 2\frac{P}{A}\sqrt{\frac{t}{\pi k \rho C}} \qquad (33)$$

$$= \Delta T_{film} = 2\frac{P}{A}\sqrt{\frac{t}{\pi k \rho C}} = 2 \times 0.22 \times 10^6 \times \left(\frac{0.5s}{\pi 1.06 W/mK \times 2000 kg/m^3 \times 2380 J/kgK} \right)^{0..5}$$

=79 K to be compared to the 17 K above.

If we take deep penetration into account, then the above film drop is reduced. We note that the line radiation amounts to 0.05 MW/m^2 rather than the total of 0.22 used above. This resulting film drop is 18 K. To this we must add the 0.17 MW/m^2 of bremsstrahlung that penetrates about 1 mm into the flibe. An approximation that neglects conduction, and is therefore an overestimate, is

$$\Delta T_{film} = \frac{P}{A}\frac{\tau}{\rho C \lambda} = 0.17 \times 10^6 \times \left(\frac{0.5s}{2000 kg/m^3 \times 2380 J/kgK \times 0.001m} \right) = 18K$$

$$\Delta T_{film} = 18K\, optical + 18K\, bremsstrahlung = 36K$$

Using the large eddy analysis, we get an estimate of the film drop of 36 K compared to the K-ε model [16] of 17 K. The two methods of calculating film temperature give some idea of the uncertainty in the calculation, which is about a factor of two in film temperature.

The heat transfer coefficient based on this analysis would be 6300 W/m^2K. A small area where the adjacent eddies converge in a down draft will have a hot

spot. Correspondingly, there will be a cold spot where the eddies converge in an upwelling. The higher predicted surface temperature will give a larger amount of evaporation. This strongly suggests more analysis, including an area-weighted analysis and, especially, experimentation.

For the flibe case at 0.22 MW/m^2, the surface temperature to use in evaporation estimates is some value between the inlet and outlet surface temperature. The inlet is 447 °C from Fig. 4. For this highly turbulent case, the surface quickly jumps by 17 °C based on the previous discussion and shown in Fig. 7. Considering the inlet temperature to be (447+17) 464 °C. The outlet temperature is 3 °C higher than the inlet owing to neutron heating. Because of strong turbulence and the neutron penetration distance of ~0.1 m, we will assume no surface enhancement of temperature. Thus, the outlet surface temperature is 467 °C. We will weight the higher end and use an effective surface temperature of 466 °C in Table 4 and 5.

Liquid metal wall

For the liquid metal cases of SnLi and Li, we assume the motion is laminar because of the stabilizing effect of the magnetic field and use the classical conduction temperature rise formula:

$$\Delta T_{film} = 2\frac{P}{A}\sqrt{\frac{t}{\pi k \rho C}} \tag{34}$$

This equation gives the temperature rise as the surface flows from inlet to outlet while being heated with a surface heat load of P/A in W/m^2. For our case, we take 10 m/s and 15 m of path length or 1.5 s of exposure. The exit surface temperature equals the entrance temperature + ΔT_{film} + $\Delta T_{blanket}$. Typically, we find the average evaporation occurs at a temperature about 3/4 of the total temperature rise between the inlet and outlet temperature: Let us call this temperature the effective temperature, T_{eff}, i.e.,

$$T_{eff} = T_{inlet} + \tfrac{3}{4}(\Delta T_{film} + \Delta T_{blanket}) \quad (35)$$

For flibe $T_{eff} = T_{inlet} + \Delta T_{film} + \tfrac{3}{4}\Delta T_{blanket}$ (36)

Table 5

Summary temperatures for liquid walls

	Flibe	SnLi	Li
ΔT_{film}, °C	17	38	22
$T_{effective}$ °C (T-allowed from edge plasma analysis)	466 (520)	577 (630)	365 (410)

The average evaporative flux from the wall for flinabe at 0.22 MW/m^2 and a surface temperature of 466 °C is 1.4×10^{19} $m^{-2}s^{-1}$.

The average evaporative flux from the wall for SnLi at 0.22 MW/m^2 and a surface temperature of 577 °C is 1.3×10^{20} $m^{-2}s^{-1}$. The inlet temperature is 447 °C, for flibe and 542 °C for SnLi and the exit surface temperatures are 467 °C and 588 °C, respectively.

The predicted temperature of the liquid wall owing to radiation heating is lower than the allowed temperature due to impurity contamination from evaporation. The inlet temperature of the liquid wall apparently can be increased, which will improve the thermal conversion efficiency.

Table 6

Properties used for candidate liquids

Liquid	C, J/kgK	ρ, kg/m^3	k, W/mK
Flibe/flinabe	2380	1900	1.06
Li	4360	450	53*
SnLi	318	6000	40 *
PbLi	160	8700	15*
Ga	380*	5900	60*
Sn	230*	5700	35 *

*500 C°

Divertor design

The plasma lost across the separatrix flows along open field lines until it strikes the divertor surface as shown in Fig. 1 (expanded view in Fig. 10). We plan to remove heat by injecting a set of high-speed (up to 100 m/s) jets at a small angle to the magnetic flux that guides the plasma flow. The jets are shown in a side-view and an end-view in Fig. 11. The jets can be made to break up into droplets if desired.

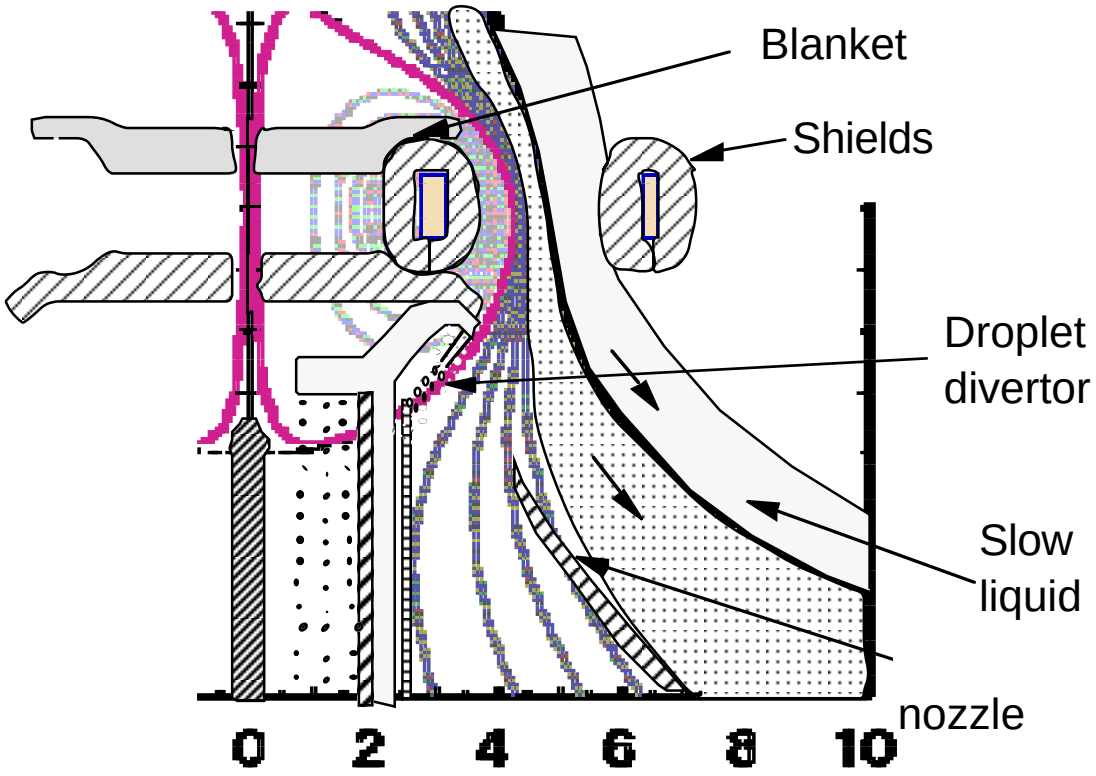

Fig. 10. The jets in the divertor are shown at 5° to the flux.

A vertical riser tube brings liquid up to an inner and an outer set of spray nozzles. These nozzles spray many rows of small jets (~0.5 mm dia) or droplets (~1 mm dia) to intercept the edge plasma. They carry away heat and provide surface area for condensation of evaporated material. The insulator must be protected from direct particle bombardment either by a sufficiently dense stream or a low conductivity film on the surface.

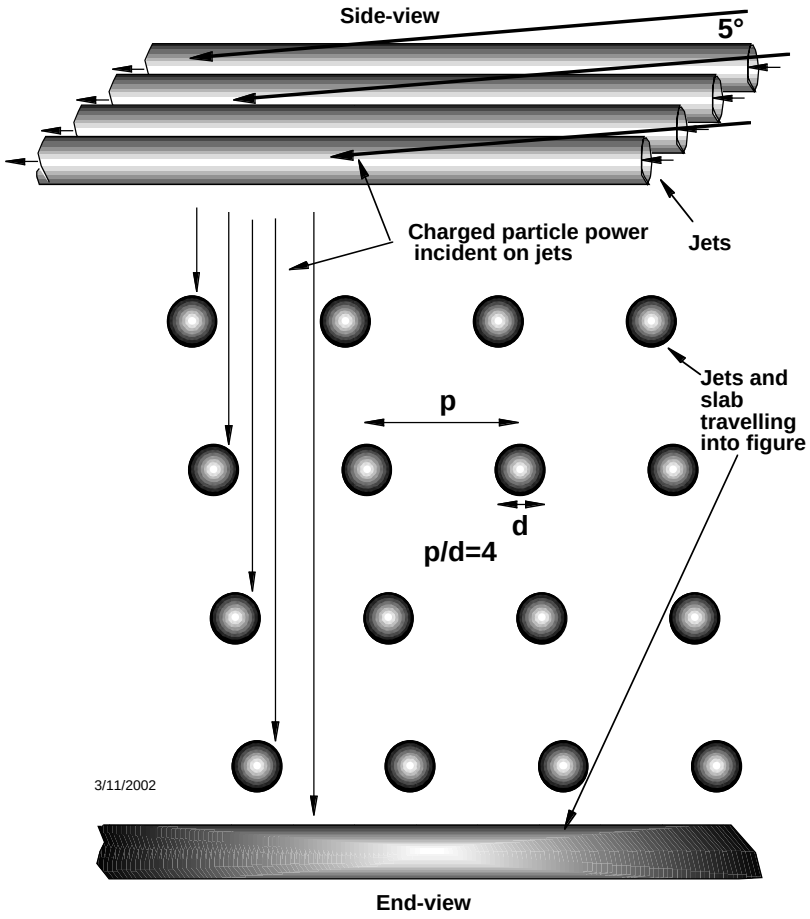

Fig. 11. Side-view and end-view of jets in the divertor are shown at 5° to the flux.

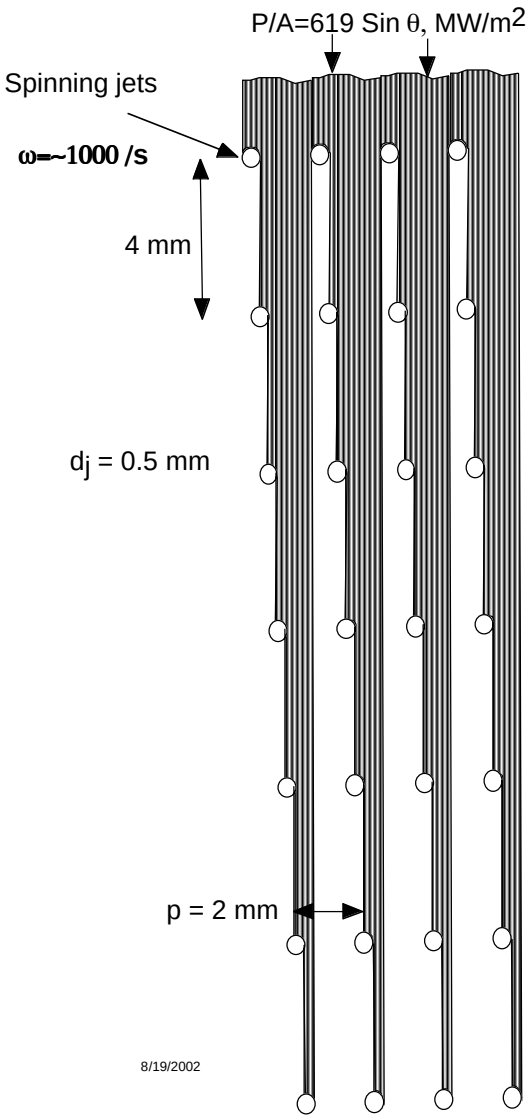

Fig. 12. The jets are shown with a pitch to diameter ratio of 4. Seven rows of these jets are needed to intercept all the power.

The distance at the midplane of the separatrix (R=0) and the secondary (inactive) separatrix (R=6.0015 m) is 1.5 mm. This flux tube at the jet divertor becomes 6 mm wide (at R=3 m, z=-12 m). If the plasma leaking across the separatrix were to completely fill this 1.5 mm flux tube, all the power would flow to the divertor at the bottom. However, the calculated edge plasma profile has an e-folding width of approximately 7 mm. We estimate about 40% will flow out the top and through the aperture where the retractable electrode is shown in Fig. 1. The

retractable electrode would be removed during normal operation after start-up. The plasma flowing through this aperture would go into a large tank with sufficient room to spread out the heat. This needs to be analyzed in future design studies.

Sixty percent of the 546 MW of leakage power, or 328 MW, is estimated to flow downward. The 7 mm wide plasma at the mid plane expands by a factor of four (6 mm / 1.5mm) to 28 mm at the divertor, whose area is (2π 3 m x 28 mm) 0.53 m^2. The 328 MW flowing into the bottom divertor then produces a power density of 619 MW/m^2 over the 28-mm wide flux tube. In future designs, the lower divertor may be expanded to carry the flux tube out to a larger area as mentioned for the upper flux tube, thereby lowering the large power density in the present case. A factor of two expansion of the flux tube width together with a 5° inclination to the field would give a 27 MW/m^2 power density on the liquid surface. This becomes manageable with jets, which lower the effective heat flux by a factor of π to 8.6 MW/m^2 by averaging over the spinning jet surface.

We now ask what are the evaporation rates for a liquid slab divertor and a jet divertor inclined at a small angle to the flow for a power density of 619 MW/m^2. The results for a slab inclined at 5°–the smallest angle that seems possible–are shown in Fig. 13. With a flow speed of 100 m / s, the average flux for flibe is 6×10^{27} $m^{-2}s^{-1}$ and 4×10^{22} $m^{-2}s^{-1}$ for SnLi. T_{in} = 673 K and T_{out} = 2249 K for flibe and T_{in} = 723 K and T_{out} = 1118 K for SnLi. The flibe case for slab geometry results in surface temperatures beyond the limits of validity of the analysis but is kept for comparison.

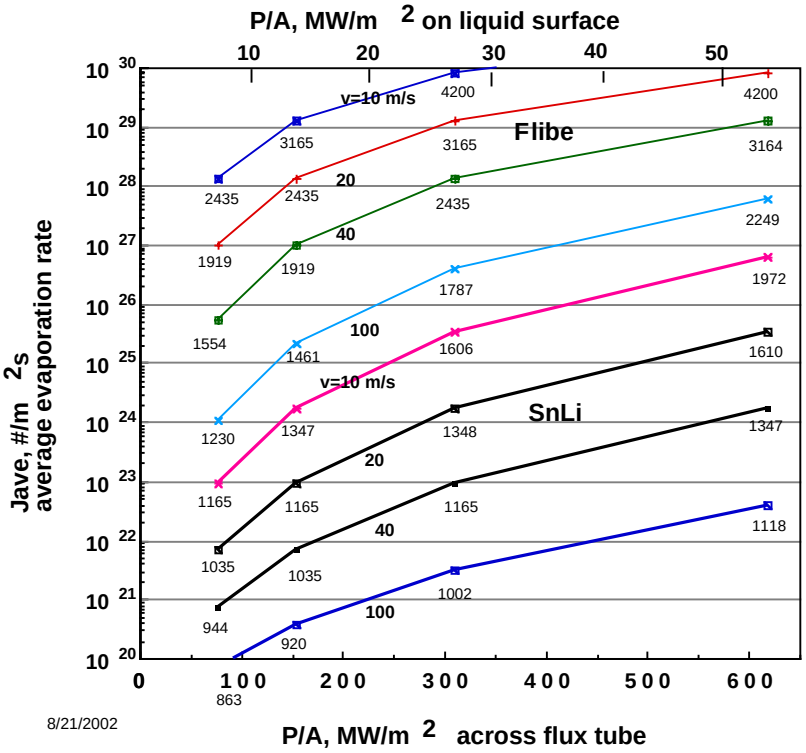

Fig. 13. Evaporation for a slab of liquid is shown. Exit temperatures are shown in Kelvin.

For four rows of jets (p / d=4) as shown in Fig. 12, the analysis shows a reduced evaporation. The results summarized in Tables 7 & 8 are 1.74×10^{23} $m^{-2}s^{-1}$ for flinabe for 100 m / s jets and 8.89×10^{24} $m^{-2}s^{-1}$ for 40 m / s jets. For SnLi the evaporation rate for 100 m / s jets is. 2.39×10^{19} m^{-2} s^{-1} and for 40 m / s jets is 1.77×10^{20} m^{-2} s^{-1}. The surface temperature at the exit for the first row is 1175 K for 100 m / s and 1466 K for 40 m / s flinabe. For SnLi the surface temperature at the exit for the first row is 849 K for 100 m / s and 922 K for 40 m / s jets. The substantial reduction of the evaporative flux compared to the slab is due to the reduction by a factor of π in average power. Exposing all sides to the incident power results in a factor of π lower temperature rise. The surface temperature appears in the exponent of the evaporation equation.

In the next section we show that the flux of impurities into the divertor are limited to $2x10^{23}$ (particles / m^2 s). The 100 m / s flibe jets meet this criterion in that the evaporation is less than $2x10^{23}$ (particles / m^2 s) but not for the 40 m / s case. The SnLi jets easily meet this criterion. For the slab, the flibe does not meet this criterion even when the flux is expanded by a factor of 8. The SnLi slab meets this criterion only at a speed of 100 m / s. At 40 m / s, the flux must be expanded by a factor of two.

Table 7

Evaporation from spinning jets

100 m / s injection speed

			Flibe		SnLi	
Row # n	P / A, MW / m^2	1 / 2x0.785* $(1-.25)^{n-1}$	J_{jet}, 10^{23} / m^2s	J_{net}	J_{jet}, 10^{19} / m^2s	J_{net}
1	197	0.3925	4.375	1.717	4.55	1.786
2	98.5	0.2944	0.0222	0.0065	0.574	0.169
3	98.5	0.2208	0.0222	0.0049	0.574	0.127
4	98.5	0.1656	0.0222	0.0037	0.574	0.095
5	98.5	0.1242	0.0222	0.0028	0.574	0.071
6	98.5	0.0931	0.0222	0.0021	0.574	0.053
7	98.5	0.0699	0.0222	0.0016	0.574	0.040
Total				1.74		2.39

*The factor 1 / 2 accounts for half of the evaporation being away from the divertor and the jet area of πd is a fraction of the total area; πd / p =0.785 for p / d=4.

Table 8

Evaporation from spinning jets

40 m / s injection speed

			Flibe		SnLi	
Row # n	P / A, MW / m^2	1 / 2x0.785 $(1-.25)^{n-1}$	J_{jet}, 10^{25} / m^2s	J_{net}	J_{jet}, 10^{20} / m^2s	J_{net}
1	197	0.3925	2.25	0.883	3.98	1.56
2	98.5	0.2944	0.0064	0.00188	0.195	0.057
3	98.5	0.2208	0.0064	0.00141	0.195	0.043
4	98.5	0.1656	0.0064	0.0011	0.195	0.032

5	98.5	0.1242	0.0064	0.00079	0.195	0.024
6	98.5	0.0931	0.0064	0.00059	0.195	0.018
7	98.5	0.0699	0.0064	0.00044	0.195	0.014
Total				0.889		1.77

Impurity Contamination

The plasma beyond the magnetic separatrix shields the core plasma from the impurities that evaporate from the liquid wall. Here we discuss the modeling of this scrape-off layer (SOL) plasma and present results on shielding effectiveness. With respect to the liquid first-wall, the maximum flux of impurities that the SOL plasma can shield then determines the allowable surface temperature of the liquid. The surface is heated by a combination of bremsstrahlung and line radiation from the core and edge region (see Table 2). The heat flux to the divertor region is also important, because it defines what peak heat flux must be tolerated by the divertor.

We use the 2-D UEDGE transport code to calculate self consistent hydrogenic and impurity plasma profiles. The initial model for the edge plasma considers the thin annulus of the edge region as a long-thin plasma slab. The X-points in the poloidal magnetic flux (see Fig. 1) are taken to be 10 m apart, and a divertor leg region of 2 m is used at each end. Because the toroidal magnetic field at the edge of a spheromak is small compared to the poloidal field, we take the B-field to have only a poloidal component. We assume that the divertor leg regions can be designed to give low recycling of the hydrogen plasma, perhaps by drawing these field lines into a large dump tank. Thus, the hydrogenic recycling coefficient at the divertors is assumed to be R_h=0.25. At the separatrix, the density of the hydrogenic species (a 50/50% mixture of deuterium and tritium) is taken to be $5x10^{19}$ m^{-3}, and power into the SOL is taken as 1.5 MW/m^2 divided equally between the ion and electron channels. The anomalous radial diffusion coefficients arising from plasma turbulence is 0.33 m^2/s for density, and 0.5 m^2/s for electron and ion thermal energies.

The calculated radial plasma profiles at the outer midplane are shown in Fig. 14. The scale length of the density, n_i and electron temperature, T_e, are very similar, both with a 1/e width of 8 mm. The ion temperature has a characteristic high-temperature tail because the ion parallel thermal conductivity is much lower than that of the electrons.

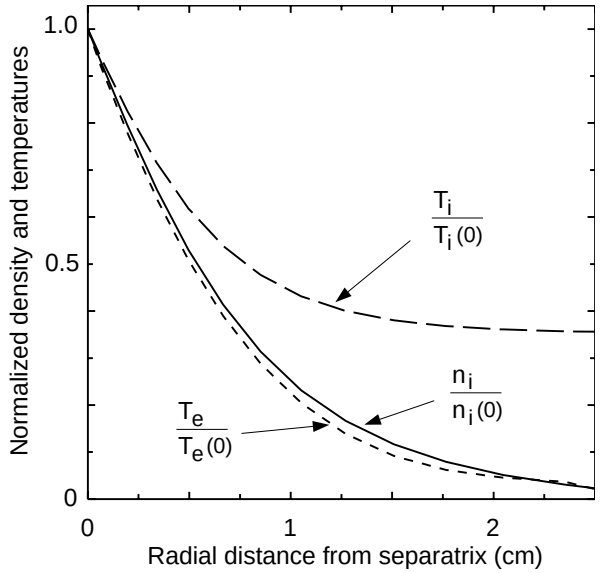

Fig. 14. Radial profiles of ion density and electron and ion temperatures. Values at the separatrix are $n_i(0)=5\text{x}10^{19}$ m^{-3}, $T_e(0)=676$ eV, and $T_i(0)=702$ eV. The input power from the core is 1.5 MW / m^2.

The impurity gas coming from the liquid wall is modeled as a uniform flux along the radial boundary at r=6.025 m (which is 2.5 cm beyond the separatrix edge) at a temperature of 1 eV. More details on the transport model and the sensitivity of results for various assumptions in given in Ref. [19]. The impurities have the same anomalous radial diffusion coefficients as the hydrogenic species. The impurity ions that return to the side wall and those reaching the divertor plate through axial flow are assumed to be mostly reabsorbed into the liquid with a small recycling coefficient of $R_{imp}=0.25$. Values of $R_{imp}<0.5$ produce very similar results. We consider two impurity gas species, lithium and fluorine. Lithium is from either a pure lithium wall or from a tin-lithium wall, which evaporates nearly all lithium. The second impurity gas considered is fluorine, which comes

from the molten salts flibe or flinabe. Because fluorine has the highest charge of the atoms in these salts, it has the lowest allowable concentration at the core edge. The resulting impurity concentrations at the core edge are shown in Fig. 15.

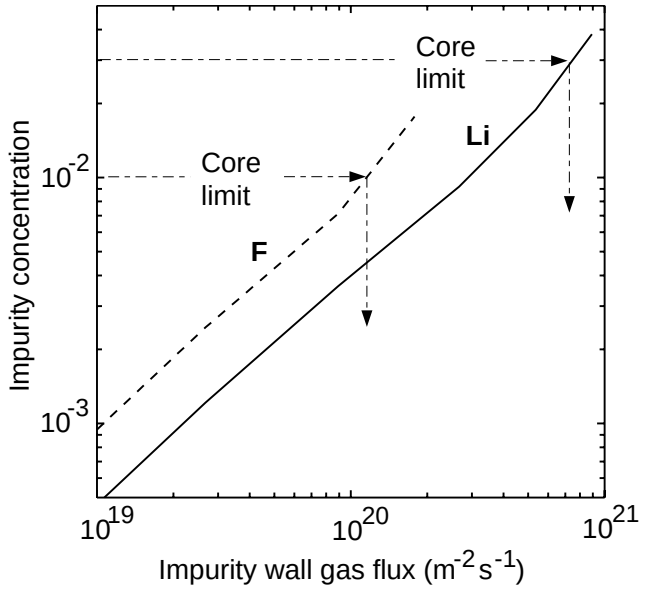

Fig. 15. Concentration of impurities (n_{imp} / n_e) at the separatrix for various liquid wall impurity gas fluxes distributed uniformly along the wall located 25 mm outside the separatrix.

Data from the vapor pressure of the various liquids versus temperature (see Fig. 5) is then used with a simple model to calculate the vapor flux. Using the limits of flux noted in Fig. 15, we arrive at the following wall temperature limits for three materials:

Table 9.
Maximum surface temperatures of liquid walls
based on acceptable core impurity levels.

Material	Lithium	Tin-lithium (80/20)	Flinabe/Flibe
Surface Temp. °C	410	630	520

The heat flux at the divertor plate is very large in this simple slab model since it does not include any expansion of the magnetic flux surfaces shown in Fig. 1 & 10. For the cases considered here, the parallel heat flux is equal to the poloidal

heat flux, because there is no toroidal B-field. As a consequence, the peak flux is approximately 1.7 GW/m^2.

This UEDGE result can be compared with the analysis presented earlier. There the flux tube area expanded from 7 mm by a factor of 4 to 28 mm. Allotting for this increase in area, the UEDGE peak heat flux scales by 1.7/4 to 425 MW/m^2, which is reasonably consistent with the Table 4 value of 546 MW/m^2.

Sputtering and evaporation set the temperature limit of the divertor surfaces. The latter limit involves the sheath superheat phenomenon, as studied for tokamaks [20, 21]. Based on those studies, a rough evaporation-based limit for the present purposes is set by the condition that the evaporating impurity flux is approximately equal to the incoming hydrogen ion flux [15, 16]. This flux ratio is, G = (impurity atom flux)/(hydrogen ion flux). When G >> 1, (exact limit depending on surface material, flow velocity, and plasma parameters) the sheath collapses and runaway overheating of the surface occurs.

For our base-case of a low-recycling divertor, the peak hydrogen ion flux is $2x10^{24} \sin\theta_\tau$ ($particles/m^2 s$), where θ_τ is the tilt angle that the divertor stream makes with the B-field; $\theta_\tau = 5^o$ for the design here. Thus, the rule of G=1 implies that the maximum impurity flux is $2x10^{23}$ ($particles/m^2 s$). From curves of evaporative flux versus surface temperature for different materials shown in Fig. 5, such a flux corresponds to the following temperatures: for Li, T=580 ^oC; flibe/flinabe, T=740 C; for SnLi, T=840 C, and for Sn, T=1380 C. (For lithium, the sputtering limit is likely to be more restrictive). These results can be compared to those predicted from heat transfer. For flibe, the evaporative flux predicted from heat transfer with rotating jets was $1.7x10^{23}$ ($particles/m^2 s$) for the 100 m/s flibe jet case. This case may be workable, but this subject needs more study.

For our base-case, the divertor surface is heated by a peak heat flux of $1x10^3 \sin\theta_\tau$ (MW/m^2) with a width of $0.7/\sin\theta_\tau$ (cm). The peak temperature of the surface then depends on the conductivity of the liquid, which can be considerably enhanced by turbulence, especially for low conductivity molten salts flibe and flinabe. Such an analysis is described in section, **Liquid Wall Design.**

Tritium breeding analysis

The potential for tritium breeding is assessed in the spheromak, shown in Figure 1. The radial blanket consists of 0.5 m thick fast-flowing liquid layer followed by ~0.5 m thick slow-flowing liquid layer. Flinabe is considered in the present assessment, but a comparison of the adequacy of tritium breeding is also made for Flibe. A design goal is to eliminate the presence of any neutron multiplier (e.g. beryllium) other than that already in the liquid in the radial blankets, shown in Fig 1 due to radiation damage lifetime and complexity, as well as resource concerns for beryllium. However, the top and bottom blankets could be designed to be dedicated regions to supplement any additional tritium such that tritium self-sufficiency is achieved in the spheromak with a possibility of utilizing beryllium as a multiplier in these regions. Geometrically, the top and bottom regions occupy ~7.5% each of the 4π of the solid angle, while the radial blanket covers the remainder (~85%).

Table 10 shows the options considered in the present assessment. It was shown that lithium-6 enrichment of 50% or higher is needed with flinabe, while enrichment of ~25% is adequate in the flibe case.

Table 11 gives the total tritium breeding ratio (TBR) and the contribution from each blanket when flinabe is considered as the liquid breeder (design option I). As shown, without beryllium in the top and bottom blankets, the TBR is marginal (TBR ~1.05). There is a risk that TBR may fall below unity if more accurate 3-D calculations are made and account taken for nuclear data uncertainties. The TBR improves upon the utilization of a front Be zone in the top

and bottom blankets. In this case, a TBR with comfortable margin is achieved. The TBR is ~ 1.12 when 100 mm thick beryllium zone is used in the top and bottom blankets and is ~1.15 with 200 mm Be zone.

Table 12 gives the corresponding tritium breeding capability in case the Flibe (25% Li-6) is used instead. The TBR is larger than with flinabe by ~11-13% (with Be in top and bottom blankets) and by ~15% (with no Be in top and bottom blankets).

Design option III (using Li-Pb in the top and bottom blankets while Flinabe (or Flibe) is used in the radial blanket) does not offer significant improvement in TBR, as shown in Table 13.

Table 10
Options Considered in Evaluating Tritium Breeding

	Option I	**Option II**	**Option III**
Radial Blanket (No Beryllium)	Flinabe (50% Li-6)	Flibe (25% Li-6)	Flinabe or Flibe
Top Blanket	Flinabe (50% Li-6)	Flibe (50% Li-6)	Li-Pb (90% Li-6)
Bottom Blanket	*No Beryllium* *10 cm Be zone* *20 cm Be Zone*	*No Beryllium* *10 cm Be zone* *20 cm Be Zone*	

Table 11

Total TBR with Flinabe and Contribution from Various Blankets

(Option I)

Blanket Location	TBR	Contribution
Radial Flinabe Wall/Blanket (No Beryllium)	0.897	~85%[1] ~80%[2] ~78.3%[3]
Top Flinabe Blanket *No Beryllium* *100 mm Be Zone* *200 mm Be Zone*	 0.078 0.111 0.124	 ~7.5% ~10% ~10.8%
Bottom Flinabe Blanket *No Beryllium* *100 mm Be Zone* *200 mm Be Zone*	 0.078 0.112 0.125	 ~7.5% ~10% ~10.9%
Total TBR *No Beryllium* *100 mm Be Zone* *200 mm Be Zone*	 *1.05* *1.12* *1.146*	

1 No Be in Top and Bottom Blankets

2 100 mm Be zone in Top and Bottom Blankets

3 200 mm Be zone in Top and Bottom Blankets

Table 12

Total TBR with Flibe and Contribution from Various Blankets

(Option II)

Blanket Location	TBR	Contribution
Radial Flibe Wall / Blanket (No Beryllium)	1.032	~85%[1] ~81.5%[2] ~80.6%[3]
Top Flibe Blanket *No Beryllium* *100 mm Be Zone* *200 mm Be Zone*	 0.089 0.118 0.124	 ~7.5% ~9.3% ~9.7%
Bottom Flibe Blanket *No Beryllium* *100 mm Be Zone* *200 mm Be Zone*	 0.089 0.117 0.125	 ~7.5% ~9.2% ~9.7%
Total TBR *No Beryllium* *100 mm Be Zone* *200 mm Be Zone*	 *1.21* *1.267* *1.281*	

1 No Be in Top and Bottom Blankets

2 100 mm Be zone in Top and Bottom Blankets

3 200 mm Be zone in Top and Bottom Blankets

Table 13
TBR with Flinabe or Flibe Breeder in Radial Blanket
And LiPb in Top and Bottom Blankets (Option III)

Blanket Location	TBR	Contribution
Radial Blanket (Flinabe) Radial Blanket (Flibe) (No Beryllium)	0.897 1.032	~80.8% (~82.8%)
Top LiPb Blanket	0.107	~9.6%[1]- ~8.6%[2]
Bottom LiPb Blanket	0.107	~9.6%[1]- ~8.6%[2]
Total TBR: *With Flinabe* *With Flibe*	*1.111* *1.246*	

1: With Flinabe in Radial Blanket…… 2: With Flibe in Radial Blanket

Conclusions and discussion

This study examines a steady-state spheromak with a flowing liquid wall. We are sufficiently encouraged by the results to recommend further work on the concept if the core plasma energy confinement database improves. The database for spheromaks is reviewed in Ref. 22 and 23. However, for flibe, the divertor evaporation is high (marginally meets our criterion) even with high speed jets (100 m/s). The advantages of the simpler reactor embodiment of the spheromak (without toroidal coils and liquid walls replacing most of the solid first wall) are impressive.

Inconsistencies needing resolution or improved performance are:

- Evaporation from the walls, while high, is acceptable with some margin according to our analysis and criterion. Therefore, the temperature can be increased according to the analysis. The film-drop calculation used 0.22 MW/m^2 surface heat load. Better estimates of surface temperature are needed. This requires better analysis and experiments on turbulent heat transfer.
- The evaporation in the divertor seems high but might be acceptable. Even when the divertor is inclined at a small angle, the power density on the liquid is still very large, resulting in very large evaporation rates. The use of spinning jets to average the power over the jets' surface allows handling much higher divertor heat load. The divertor needs further study and ways to reduce the heat loads by perhaps expanding the flux surface a factor of two or so.
- The gun threading magnetic flux is unusually small (1/1000 times the spheromak flux). Will this be realistically achievable?
- The plasma parameters need to be estimated more accurately with more detailed modeling.
- We should learn how to breed tritium without enriching the lithium and without adding solid beryllium to the blankets at the top and bottom.

Acknowledgments

This work is part of the Advanced Power Extraction (APEX) project sponsored by DOE Office of Fusion Energy Science. Support by Kyoto University, Institute of Advanced Energy is appreciated. *Work performed under the auspice of the U.S. Department of Energy by University of California Lawrence Livermore National Laboratory under Contract W-7405-Eng-48.

References

1. P. M. Bellan, Spheromaks, Imperial College Press, London, 2000.
2. R. L. Hagenson and R. A. Krakowski, Fusion Technology **8**, 1606 (1985).
3. L. J. Perkins, unpublished work on spheromak reactor designs (1995).
4. T. K. Fowler, D. D. Hua, E. G. Hooper, R. W. Moir and L. D. Pearlstein, "Pulsed spheromak fusion reactors," Comments on Plasma Physics and Controlled Fusion, Comments on Modern Physics, Vol 1 Part C 83-98 (1999).
5. E. B. Hooper and T. K. Fowler, "Spheromak reactor: Physics opportunities and issues," Fusion Tech., **30**, 1390 (1996).
6. P. F. Peterson, UC Berkeley, private communications in a briefing (March 4, 2001).

6a E. B. Hooper, et al., "MHD Equilibria in a Spheromak Sustained by Coaxial Helicity Injection," Nuclear Fusion 39 (1999) 863.

7. T. K. Fowler and E. B. Hooper, "Advanced Spheromak Fusion Reactor", submitted to the 8th International Conference on Emerging Nuclear Energy Systems (Obninsk, Russia) June 24-28, 1996. Lawrence Livermore National Laboratory Report UCRL-JC-124363, June 19, 1996.
8. R. W. Moir et al., "Thick liquid-walled field-reversed configuration–magnetic fusion power plant," Fusion Technology **39**, 758-767 (2001).
9. J. Wesson, Tokamaks, Clarendon Press, Oxford (1887).
10. T. K. Fowler, D. D. Hua and B. W. Stallard, "Simulations of SSPX Sustainment -- Toward a Standard Model for Spheromaks," UCRL-ID141998, Jan. 12, 2001.

11. C. W. Barnes, T. R. Jarboe, G. J. Marklin, S. O. Knox and I. Henins, Phys. Fluids B **2**, 1871 (1999).
12. M. A. Abdou et al. “On the exploration of innovative concepts for fusion chamber technology,” UCLA-ENG-99-206 (1999). Fusion Engineering and Design **54** (2001) 181-247.
13. S. Cantor, D. S. Hsu, and W. T. Ward, "Vapor Pressures of Fluoride Melts," in Reactor Chem. Div. Ann. Progr. Rept., Oak Ridge National Laboratory, Oak Ridge, Tenn., ORNL-3913, pp. 24-26 (1965). For Flibe.
14. D. R. Olander, G. Fukuda, D. F. Baes, Jr. (2002), “Equilibrium Pressures Over BeF_2-LiF (Flibe) Molten Mixtures,” Fusion Science and Technology **41**(2):141-150.
15. S. Smolentsev, UCLA, private communications, November 13, 2001.
16. S. Smolentsev, M. Abdou, N. Morley, A. Ying, T. Kunugi, “Applications of the “K-ε” model to open channel flows in a magnetic field,” Int. J. Engineering Science**, 40/6**, 693-711 (2002).
17. T. Kunugi, S. Satake, A. Sagara, "Direct numerical simulation of turbulent free-surface high Prandlt number fluid flows in a fusion reactor," Nuclear Instruments and Methods in Physics Research, **A464** (2001) 165-171.
18. T. Kunugi, University of Kyoto, private communications (May 2002).
19. T. D. Rognlien and M. E. Rensink, "Impurity transport in edge plasmas with application to liquid walls." Phys. Plasmas **9** (2002) 2120.
20. J.N. Brooks and D. Naujoks, “Sheath superheat transmission due to redeposition of thermally emitted material,” Phys. Plasmas, Vol**. 7** (2000) 2565.

21. D. Naujoks and J.N. Brooks, "Combined sheath and thermal analysis of overheated surfaces in fusion devices," J. Nucl. Mater., Vol. **290-293** (2001) 1123.

22 H. S. McLean, S. Woodruff, E. B. Hooper, R. H. Bulmer, D. N. Hill, C. Holcomb, J. Moller, B. W. Stallard, R. D. Wood, Z. Wang., Phys. Rev. Letters **88**, 125004 (2002).

23 D. N. Hill, R. H. Bulmer, B. I. Cohen, E. B., Hooper, H. S. McLean, J. Moller, L. D. Pearlstein, D. D. Ryutov, B. W. Stallard, R. D. Wood, S. Woodruff, IAEA Conf., Lyon, France Oct. 2002, paper EX/C1-3.